JTTEE 3:179-183

Analysis of the Two-Phase Flow in a de Laval Spray Nozzle and Exit Plume

Y.-M. Lee and R.A. Berry

One method used in spray forming and coating technology involves transonic/supersonic gas-droplet two-phase flows through a de Laval nozzle and subsequent subsonic freejet flow from the nozzle to the sprayed surface. To the first-order approximation, this complex phenomenon can be treated in a quasi-one-dimensional manner to simulate the entire converging-diverging nozzle flow field (with particle injection at the throat) as well as the plume (freejet) region. The basic numerical technique and computer model solve the steady gas field equations through a conservative variable approach and treat the droplet phase in a Lagrangian manner, with full aerodynamic and energetic coupling between the droplets and the transport gas handled via source terms. These analyses are simple and economical to execute. The one-dimensional models are valuable in constructing algorithms for automated process control. Finally, these one-dimensional models give direction to two- and three-dimensional simulations and serve as a test bed for models based on particle dynamics and energetics.

1. Introduction

THE controlled atomization process is a thermal spray process that atomizes liquid metals in the flow of a de Laval nozzle (Ref 1). Modified Idaho National Engineering Laboratory (INEL) quasi-one-dimensional nozzle and plume computer codes (Ref 2) were used to examine the experimental data and nozzle configurations at MSE, Inc. During this test period, the computer codes were modified and simulation runs were performed to support the new pressurized nozzle design and data analyses. This paper describes the modeling effort, the modification and improvement to the code, and the simulation results.

2. Modeling Methodology

The process of spray-casting technology involves transonic gas-particle (droplet) flows through de Laval nozzles and subsonic freejet flow from the nozzle to the sprayed surface. Detailed derivation of the modeling equations can be found in References 2 and 3; this section presents a description of the equations used.

2.1 *Flow Conservation Equations*

Flow in a duct having a slowly varying cross section, where the duct height is small compared with the radius of curvature of the axis of the duct, is termed a quasi-one-dimensional flow. The quasi-one-dimensional flow of a particle-laden gas in a duct of uniformly varying cross-sectional area where a typical control volume (computational cell) is bounded by the walls of the duct and by stations 1 and 2 is shown in Fig. 1. The entire flow-field is divided (axially) into such control volumes. For the control volume shown in Fig. 1, the mass conservation equation for steady gas flow is

$$\rho_2 u_2 A_2 = \rho_1 u_1 A_1 \qquad \text{(Eq 1)}$$

where ρ is gas density, u is gas velocity, and A is cross-sectional area, and the subscripts refer to stations 1 and 2. Applying the momentum principle for the control volume in terms of the flow properties gives (Ref 3):

$$p_2 A_2 + \rho_2^2 A_2 = p_1 A_1 + \rho_1 u_1^2 A_1 + \frac{1}{2}(p_1 + p_2)(A_2 - A_1) + \Delta \dot{M}_p - F_{wx} \qquad \text{(Eq 2)}$$

where p is the gas pressure at stations 1 and 2, $\Delta \dot{M}_p$ is the "source" term for momentum due to the presence of the particles (evaluated from the equations of motion for the particles in the flow field), and F_{wx} is the shear force at the wall opposing fluid motion. The energy conservation principle for the control volume is

$$\rho_2 u_2 A_2 (h_2 + \frac{1}{2}u_2^2) = \rho_1 u_1 A_1 (h_1 + \frac{1}{2}u_1^2) + \Delta \dot{E}_p + \dot{Q} \qquad \text{(Eq 3)}$$

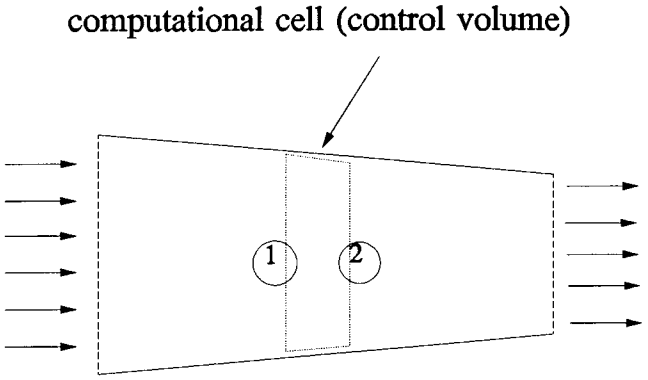

Fig. 1 Computational cell configuration

Key Words: de Laval nozzle, modeling, nozzle design, spray forming, spray casting

Y.-M. Lee, MSE Inc., Butte, MT 59702, USA; and **R.A. Berry,** EG&G Idaho, Idaho Falls, ID 83415, USA

where h is the enthalpy of the gas at stations 1 and 2, $\Delta\dot{E}_p$ is the "source" energy due to the presence of the particulate phase (evaluated from the equations of energy for the particles in the flow field), and $\dot{Q}$ is the thermal energy added to the flow per unit time between stations 1 and 2 (i.e., heat transfer from the walls).

In terms of the new dependent variables X, Y, and Z, the governing equations (Eq 1 to 3) can be written as:

$$X_2 = X_1 \tag{Eq 4}$$

$$Y_2 = Y_1 + \Delta\dot{M}_p + \left(\frac{p_1 + p_2}{2}\right)(A_2 - A_1) - F_{wx} \tag{Eq 5}$$

$$Z_2 = Z_1 + \Delta\dot{E}_p + \dot{Q} \tag{Eq 6}$$

where:

$$X = \rho\dot{u}A \tag{Eq 7}$$

$$Y = pA + \rho u^2 A = pA + Xu \tag{Eq 8}$$

$$Z = (h + \frac{u^2}{2})\rho uA \tag{Eq 9}$$

2.2 *Particle Source Terms*

The momentum and energy source terms for the particles are obtained by integrating the equations of particle motion and heat transfer using the velocity, pressure, and temperature fields of the gas. The Lagrangian approach is used for this integration. The particle momentum equation can be integrated between stations 1 and 2 to obtain:

$$v_2 = \sqrt{\left(\frac{\lambda\Delta x}{\tau_a}\right)^2 + v_1^2 + 2\left(\frac{\lambda\Delta x}{\tau_a}\right)u_2} - \left(\frac{\lambda\Delta x}{\tau_a}\right) \tag{Eq 10}$$

where:

$$\lambda = \frac{Re_p}{24}C_d \tag{Eq 11}$$

$$\tau_a = \frac{\rho_p D_p^2}{18\mu} \tag{Eq 12}$$

$$Re_p = \frac{\rho|u - v|D_p}{\mu} \tag{Eq 13}$$

where D_p is particle diameter, ρ_p is particle mass density, μ is gas viscosity, and Re_p is the Reynolds number based on particle diameter. The factor τ_a is the aerodynamic response time, which is defined as the time required for a particle released from rest to achieve 63% of free stream velocity (in Stokes flow, where λ = 1, $C_d = 24/Re_p$). The drag coefficient, C_d, used for Re_p <300,000 is (Ref 4):

$$C_d = \frac{24}{Re_p}(1 + 0.15Re_p^{0.687}) + \frac{0.42}{1 + 4.25\cdot 10^4 Re_p^{-1.16}} \tag{Eq 14}$$

The energy equation for a solidifying droplet in a gas stream can be approximately integrated between stations 1 and 2 in a semi-implicit manner to yield:

$$T_{p2} = \frac{T_{p1} + \dfrac{Nu\Delta x T_{g2}}{(v_1 + v_2)\tau_t} - \dfrac{12D_i^2 H\Delta x\dot{r}_i}{(v_1 + v_2)(C_p)_m D_p^3}}{1 + \dfrac{Nu\Delta x}{(v_1 + v_2)\tau_t}} \tag{Eq 15}$$

$$Nu = 2 + 0.6Re_p^{0.5}Pr^{0.333} \tag{Eq 16}$$

where Pr is the Prandtl number. The computational code is constructed to handle the flow with full coupling to the injection system dynamics and to permit calculations on in-flight droplet/particle undercooling, recalescence, and solidification.

2.3 *Plume Region*

The plume region program is based on empirical input for the entrainment rate as opposed to expansion angle. The basic equations follow.

Entrainment rate:

$$\frac{\dot{m}_x}{\dot{m}_0} = 0.32\sqrt{\frac{\rho_0}{\rho_j}}\cdot\frac{x}{D_0} \tag{Eq 17}$$

where $\dot{m}_x$ is the (cumulative) entrainment rate, $\dot{m}_0$ is the initial jet mass flow, ρ_0 is the environmental density, ρ_j is the jet gas density, and D_0 is the initial jet diameter. This entrainment rate was not measured with a two-phase jet; this is the classic result for a round jet.

Momentum:

$$\frac{\dot{m}_2}{U_2} - \dot{m}_1 = \frac{\dot{m}_p\Delta x f}{\tau_A}\left(1 - \frac{\overline{U}}{\overline{V}}\right) \tag{Eq 18}$$

where U is gas velocity, V is particle velocity, and f is a friction factor. The overbars correspond to the average values in the cell. Solving for U_2 produces:

$$U_2 = \frac{\dot{m}_1}{\dot{m}_2}U_1 + \frac{\dot{m}_p\Delta x f}{\dot{m}_2\,\tau_A}\left(1 - \frac{\overline{U}}{\overline{V}}\right) \tag{Eq 19}$$

Energy:

$$\dot{m}_2 c_2 T_2 - \dot{m}_1 c_1 T_1 - \dot{m}_e c_0 T_0 = \dot{n}\Delta x\, Nuk\ \pi\, d(T_p - \overline{T}) \tag{Eq 20}$$

where $\dot{n}$ is the particle number flow rate and $\dot{m}_e$ is the entrainment flow rate over the step δx. Equation 20 can be rewritten for T_2 as:

$$T_2 = \frac{\dot{m}_1 c_1}{\dot{m}_2 c_2} T_1 + \frac{\dot{m}_e c_0}{\dot{m}_2 c_2} T_0 + 0.67 \frac{Nu}{Nu_0} \frac{\Delta x}{\bar{V} \tau_A \mathrm{Pr}} \frac{\dot{m}_p}{\dot{m}_2} (T_p - \bar{T}) \quad \text{(Eq 21)}$$

3. Improvement of Simulation Code

The following improvements were made to the quasi-one-dimensional computer codes (Ref 2) for better simulation.

Volume fraction effects: For thicker, more concentrated sprays, the displacement of droplets/particles of the carrier gas cannot be neglected as for dilute sprays. The net effect for the gas is similar to a net reduction of the flow cross-sectional area, because the local volume fraction of gas is reduced. In the computation algorithm, this change was implemented by modifying the mass flux variable $X = \rho u A$, which in the new version becomes $X = \alpha \rho u A$, where α is the local volume fraction of gas.

Gas dynamic pressure gradient forces (buoyancy force): The pressure gradient force term may only be significant in regions of large gas accelerations, such as in the throat region of the nozzle or through the shock wave. This force is due to the pressure gradient in the gas phase, in the same manner as the buoyancy force in a quiescent fluid is due to the gravity force.

Supersonic exit conditions: Code modifications were made so that if the shock wave is pushed to the exit plane of the nozzle while the code is trying to match the exit plane pressure, the shock wave will be dispensed and the exit pressure condition will not be matched.

Subsonic flow throughout the nozzle: If a spray nozzle is driven in a manner so that the flow is not choked, the original code would not correctly simulate the nozzle/spray dynamics. A new version of the code was constructed to handle subsonic flow throughout the nozzle with full coupling to the injection system dynamics and to make possible in-flight droplet/particle undercooling, recalescence, and solidification.

New friction factor equation: An equation by Chen was used to calculate the friction factor in a closed conduit (Ref 5). The equation can be expressed as:

$$\frac{1}{\sqrt{f}} = -2.0 \log \left[\frac{\varepsilon}{3.7065 D} - \frac{5.0452}{\mathrm{Re}} \times \log \left(\frac{1}{2.8257} \left(\frac{\varepsilon}{D} \right)^{1.1098} + \frac{5.8506}{\mathrm{Re}^{0.8981}} \right) \right] \quad \text{(Eq 22)}$$

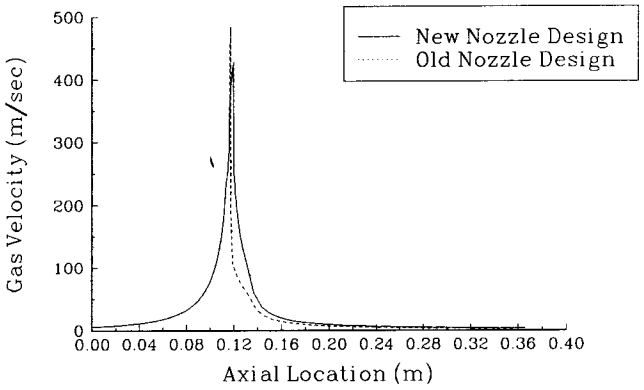

Fig. 2 Gas velocity spatial distribution

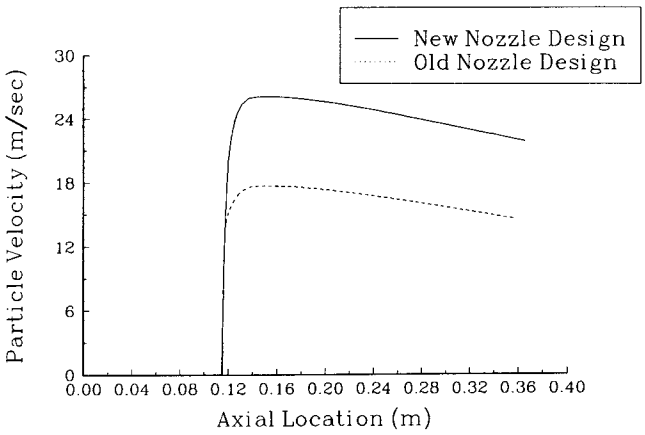

Fig. 3 Particle velocity spatial distribution

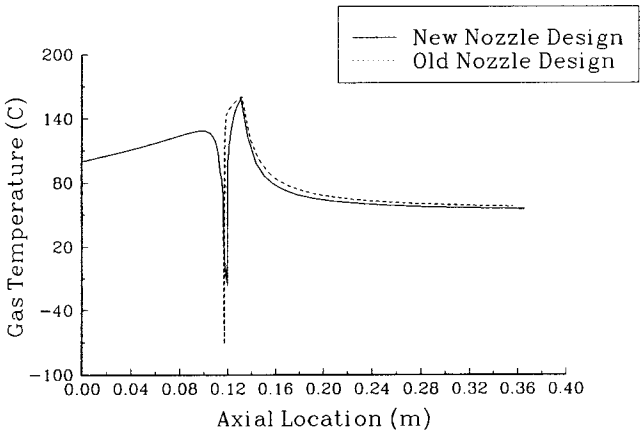

Fig. 4 Gas temperature spatial distribution

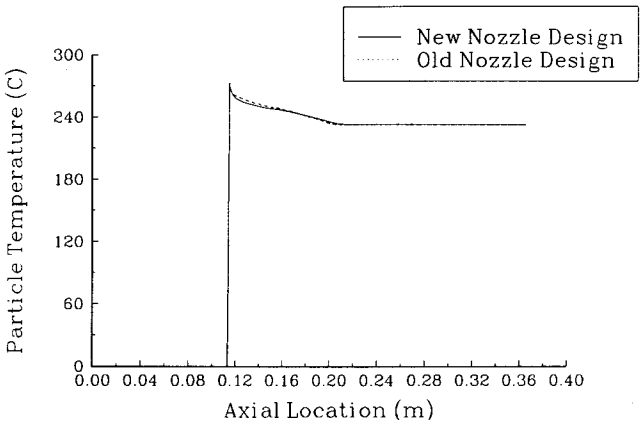

Fig. 5 Particle temperature spatial distribution

New viscosity equation: A widely used Sutherland formula (Ref 6) was adopted to calculate the viscosity of dilute gases. The final formula is

$$\frac{\mu}{\mu_0} \approx \left(\frac{T}{T_0}\right)^{1.5} \frac{T_0 + S}{T + S} \qquad \text{(Eq 23)}$$

where S is an effective temperature, called the Sutherland constant, which is characteristic of the gas.

4. Nozzle Design and Simulation

Parametric studies were performed with the quasi-one-dimensional model to estimate the importance of various parameters in the liquid-metal spray-casting process, and a series of simulations were performed to verify whether a pressurized tundish provides better control to the process. The simulation results show that the characteristics of the nozzle can be adjusted by changing the nozzle geometry. Much higher particle velocity can also be obtained by using a pressurized tundish.

Nozzle design for tin series: This design series attempted to improve the flow properties through changes in the nozzle geometry. The new design is a modified version that eliminates some undesirable design features of an earlier round nozzle design. The basic philosophy of the new design is to reduce any strong discontinuities (shock waves) and to increase the particle spray velocity. A series of computer modeling runs were performed using the old and new nozzle designs; no pressurized tundish was used. The values of parameters used are as follows (these values are suggested for future baseline testing): argon inlet pressure, 0.1314 MPa; argon inlet temperature, 100 °C; nozzle wall temperature, 272 °C; liquid tin temperature, 272 °C; and assumed particle size, 100 μm.

Figures 2 to 5 present the results of computer modeling efforts. Figure 2 shows the gas velocity distributions between the nozzle designs; the new nozzle design displays weaker shock wave and smoother velocity transition, which provides better structure protection. A normal shock wave is assumed during high inlet pressure conditions for converging-diverging nozzles (Ref 7). Figure 3 displays the particle velocity distributions between nozzle designs; the new nozzle design produces 40% higher particle velocity when particles leave the nozzle. Figure 4 shows that the new nozzle design produces a smoother gas temperature distribution in the nozzle, which provides better temperature control to the process. Figure 5 shows that the two nozzle designs deliver similar particle temperature histories; the particles start to solidify at a location less than 10.15 cm from the nozzle exit with either nozzle design. In conclusion, results from the computer modeling show that the new nozzle design yields higher particle spray velocity and smoother flow characteristics than the old nozzle design.

Pressurized tundish design: Conventional nozzle design depends on the negative pressure differential at the throat region to pull the liquid metal into the spray nozzle, which restricts the operational gas (argon) inlet pressure ranges. The pressurized tundish concept provides the freedom of almost unlimited gas (argon) inlet pressure ranges, which allows the nozzle design to be tailored to different applications. Figure 6 displays the particle velocity distributions for different argon inlet pressures. It can be seen that higher particle velocities are achieved through higher argon inlet pressures, which allows better control of the process.

Characterization study: A nozzle design, identified as 92-3B1, was compared with results from the modified one-dimensional nozzle and plume code. The relationships between the nozzle inlet and throat pressures were used for the study, with assumptions of nozzle inlet temperatures (argon) of room temperature, 300 °C, and 600 °C, and nozzle wall temperatures of room temperature, 382 °C, and 582 °C.

Figure 7 shows the throat pressure versus the inlet pressure under different temperature settings from the test data, including a transient state that cannot be modeled by the steady-state code discussed in this paper. The areas of particular interest for comparison purposes are the five clustered regions.

The modeling results show reasonable agreement with the test data, especially at the lower nozzle inlet pressure range. The one-dimensional code is limited when the three-dimensional effects in the nozzle flow become significant at the higher nozzle inlet pressures.

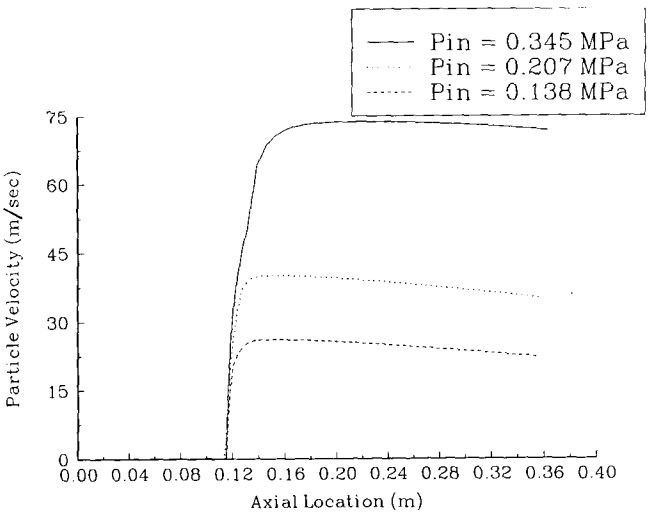

Fig. 6 Particle velocity spatial distributions with respect to three inlet pressures

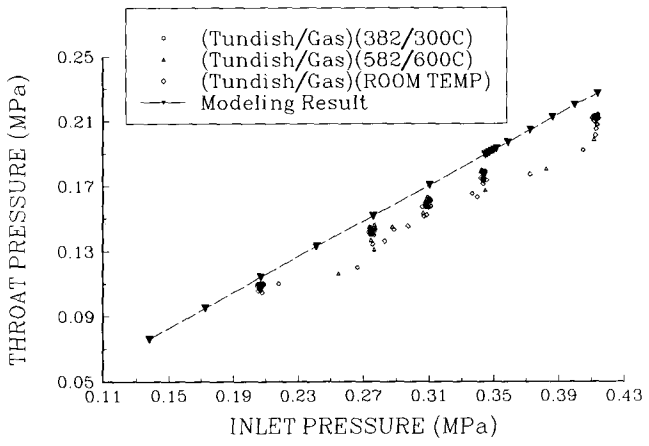

Fig. 7 Nozzle inlet and throat pressure relationship from test data and modeling results

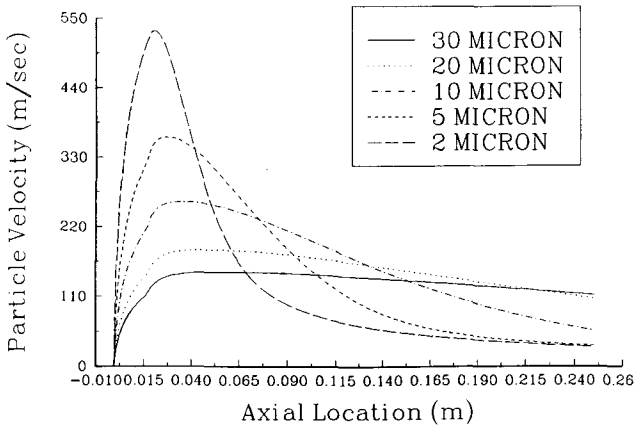

Fig. 8 Velocity spatial distribution for different particle sizes

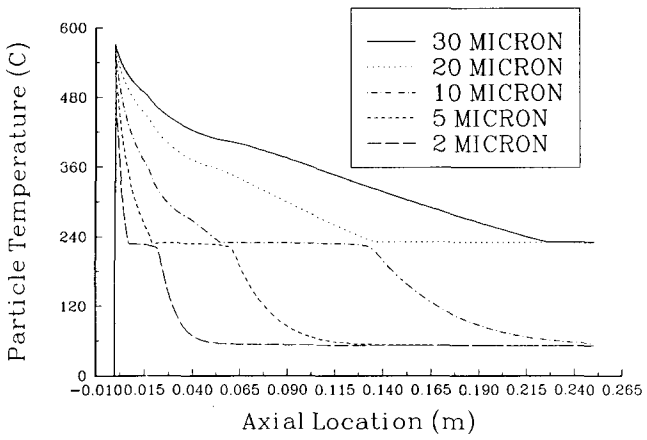

Fig. 9 Temperature spatial distribution for different particle sizes

The throat pressure does not respond quickly enough with the inlet pressure changes, and the throat-to-inlet pressure ratio does not maintain a constant value during sudden inlet pressure changes. However, the ratio returns to the steady-state value after staying at the same new inlet pressure value for a period of time. The throat pressure-to-inlet pressure ratio changes with the tundish and gas temperatures, but only slightly.

One-dimensional spray nozzle and plume examples: Figure 8 shows typical particle velocities for different particle sizes, and Fig. 9 shows particle temperatures for different particle sizes. Preliminary experimental data collected from video-recording analysis indicated that the velocities of the large particles (~200 μm) ranged from 16 to 32 m/s, with a mean of 24 m/s. The particle velocity distribution displayed in Fig. 3 was calculated for a particle size of 200 μm, which corresponds with the results of the experimental data (Fig. 8).

5. Summary and Conclusion

A quasi-one-dimensional model was developed and used in studies of the controlled atomization process. This model has yielded accurate information in the nozzle design and pressurized tundish areas in the past, and provides further credibility to the modeling principles. The model will provide more valuable information for the automated control of spray-casting processes in the future, as well as direction to the two- and three-dimensional simulations that are currently under development in the project. Further diagnostic measurements providing particle size, velocity, and temperature distribution information are needed for continued insight into the process and future improvements to the modeling process.

Acknowledgments

This work has been sponsored by the U.S. Air Force, Civil Engineering Service Agency (Tyndall AFB, Panama City, FL) and by the U.S. Department of Energy—Office of Technology Development under Contract No. DE-AC22-88ID12735.

References

1. R.J. Glovan and J.C. Tierney, Controlled Aspiration—A New Thermal Spray Process, *Thermal Spray Coatings: Research, Design, and Applications*, C.C. Berndt and T.F. Bernecki, Ed., ASM International, 1993, p 111-119
2. W. DuBroff, "Development of a Spray-Forming Process for Steel," Final Program Report, DOE-ID-10349, 1991, I-38 to I-53
3. R.A. Berry and C.T. Crowe, "Quasi-One-Dimensional Models for the Analysis of the Two-Phase Flow in a de Laval Spray Forming/Coating Nozzle and Free Jet Exit Plume," presented at Multiphase Flow Problems in Manufacturing and Production Technology, ASME Fluids Engineering Division Summer Meeting, Bethesda, MA, 1993
4. R. Clift, J.R. Grace, and M.E. Weber, *Bubbles, Drops, and Particles*, Academic Press, 1978
5. W.S. Janna, *Engineering Heat Transfer*, PWS Publishers, 1986
6. H. Schlichting, *Boundary Layer Theory*, 7th ed., McGraw-Hill, 1979
7. M.J. Zucrow and J.D. Hoffman, *Gas Dynamics*, 2nd ed., John Wiley & Sons, 1976